The Journal of Neuroscience, October 1, 1999, *19*(19):8528–8541

Ca^{2+}-Permeable AMPA Receptors and Spontaneous Presynaptic Transmitter Release at Developing Excitatory Spinal Synapses

Jeffrey Rohrbough and Nicholas C. Spitzer

Department of Biology and Center for Molecular Genetics, University of California, San Diego, La Jolla, California 92093

At many mature vertebrate glutamatergic synapses, excitatory transmission strength and plasticity are regulated by AMPA and NMDA receptor (AMPA-R and NMDA-R) activation and by patterns of presynaptic transmitter release. Both receptors potentially direct neuronal differentiation by mediating postsynaptic Ca^{2+} influx during early development. However, the development of synaptic receptor expression and colocalization has been examined developmentally in only a few systems, and changes in release properties at neuronal synapses have not been characterized extensively. We recorded miniature EPSCs (mEPSCs) from spinal interneurons in *Xenopus* embryos and larvae. In mature 5–8 d larvae, ~70% of mEPSCs in Mg^{2+}-free saline are composed of both a fast AMPA-R-mediated component and a slower NMDA-R-mediated decay, indicating receptor colocalization at most synapses. By contrast, in 39–40 hr embryos ~65% of mEPSCs are exclusively fast, suggesting that these synapses initially express predominantly AMPA-R. In a physiological Mg^{2+} concentration (1 mM), mEPSCs throughout development are mainly AMPA-R-mediated at negative potentials. Embryonic synaptic AMPA-R are highly Ca^{2+}-permeable, mEPSC amplitude is over twofold larger than at mature synapses, and mEPSCs frequently occur in bursts consistent with asynchronous multiquantal release. AMPA-R function in this motor pathway thus appears to be independent of previous NMDA-R activation, unlike other regions of the developing nervous system, ensuring a greater reliability for embryonic excitatory transmission. Early spontaneous excitatory activity is specialized to promote AMPA-R-mediated synaptic Ca^{2+} influx, which likely has significant roles in neuronal development.

Key words: Ca^{2+}-permeable AMPA receptors; NMDA receptors; developing excitatory synapses; spontaneous transmitter release; mEPSCs; receptor colocalization; presynaptic mEPSC bursts

AMPA and NMDA glutamate receptor subtypes (AMPA-R and NMDA-R) are colocalized postsynaptically at many mature central glutamatergic synapses and are activated concurrently by synaptic transmitter release (Nicoll et al., 1990). AMPA-R are used for fast excitatory signaling, whereas NMDA-R-mediated Ca^{2+} influx is believed to underlie multiple forms of developmental and activity-dependent synaptic plasticity, including long-term potentiation (LTP). Because NMDA-R are usually not functional until the postsynaptic membrane is depolarized by AMPA-R activation, the proximity and degree of coactivation of both receptors at individual excitatory synapses have important implications for function and plasticity at both developing and mature synapses.

A number of developmental studies support a predominant role for NMDA-R in initial glutamatergic transmission (Constantine-Paton and Cline, 1998; Feldman and Knudsen, 1998). NMDA-R are detected first at developing excitatory synapses in mammalian hippocampus (Durand et al., 1996; Liao et al., 1998), sensory cortex (Crair and Malenka, 1995; Isaac et al., 1997) and spinal cord (Ziskind-Conhaim, 1990), and in *Xenopus* optic tectum (Wu et al., 1996). NMDA-R synaptic currents are also more prolonged initially than at later stages (Carmignoto and Vicini, 1992; Hestrin, 1992), and NMDA-R-mediated Ca^{2+} influx may serve multiple roles in synaptic development (Sheetz and Constantine-Paton, 1994; Sheetz et al., 1997; Constantine-Paton and Cline, 1998). Functional AMPA-R expression may be induced at initially "silent" synapses by NMDA-R activation (Malenka and Nicoll, 1997). However, it remains unclear how NMDA-R provide this induction signal because transmission at immature, pure NMDA-R synapses usually is revealed only at depolarized potentials or in Mg^{2+}-free saline. Depolarizing GABA responses may have such a role in some immature neurons (Ben-Ari et al., 1997; Constantine-Paton and Cline, 1998).

Alternatively, Ca^{2+}-permeable AMPA-R may mediate Ca^{2+}-dependent developmental and plastic synaptic changes independently of NMDA-R. Ca^{2+}-permeable AMPA-R are expressed first on cultured rat hypothalamic and *Xenopus* spinal neurons (van den Pol et al., 1995; Gleason and Spitzer, 1998) and underlie mature excitatory transmission in chick cochlear nucleus (Otis et al., 1995). Synaptic AMPA-R function can be modulated directly by postsynaptic AMPA-R-mediated Ca^{2+} entry (Gu et al., 1996; Jia et al., 1996; Mahanty and Sah, 1998), but little is known about the developmental appearance of Ca^{2+}-permeable AMPA-R at embryonic synapses *in vivo*. Additionally, few studies have examined changes in patterns of presynaptic transmitter release (Gao et al., 1998; Wall and Usowicz, 1998) that may influence the contribution of AMPA-R and NMDA-R to developing synaptic responses.

We use whole-cell recordings of spontaneous mEPSCs to analyze functional properties of glutamate receptors at developing excitatory spinal synapses in *Xenopus* embryos and larvae. We

Received Jan. 29, 1999; revised July 15, 1999; accepted July 15, 1999.

We thank Dr. E. L. Gleason for insightful comments on this manuscript, I. Hsieh and S. Watt for technical assistance, Dr. P. Vincent for providing analysis software, and Dr. D. Leander of Lilly Research Laboratories, Indianapolis, IN, for the gift of GYKI 53655.

Correspondence should be addressed to Dr. Nicholas C. Spitzer, Department of Biology, 0357, University of California, San Diego, 9500 Gilman Drive, La Jolla, CA 92093-0357.

Dr. Rohrbough's present address: Department of Biology, University of Utah, 257 South 1400 East, Salt Lake City, UT 84112-0840.

find that both AMPA-R and NMDA-R are colocalized at most mature larval synapses. At embryonic stages, mEPSCs are mediated almost entirely by AMPA-R at negative membrane potentials, have larger amplitudes, and frequently occur in bursts, differing from mEPSC activity at mature stages. Furthermore, AMPA-R are permeable to Ca^{2+} from their earliest detection, suggesting that AMPA-R activation provides a pathway for Ca^{2+} influx that may serve an important role in the plasticity of developing spinal synapses.

MATERIALS AND METHODS

Spinal cord preparations. Experiments were performed on *Xenopus laevis* embryos and larvae at developmental stages between 39 hr after fertilization and 8 d of age. Animals were staged by standard morphological criteria (Nieuwkoop and Faber, 1967), and the results are grouped into three developmental categories that we refer to as embryonic, early larval, and mature larval stages. The embryonic stage is 39–40 hr after fertilization (morphological stage 31/32), which precedes hatching by ~15 hr. The early larval stage (~54 hr; stage 37/38) corresponds to the stage of hatching and the beginning of free swimming (Sillar and Roberts, 1988). Mature larvae were 5–8 d of age.

Spinal cords were dissected and secured for recording by using methods similar to those reported previously (Rohrbough and Spitzer, 1996). Larvae were decapitated in recording solution containing 0.1 μg/ml TTX (see below) and pinned into small Sylgard (Dow Corning, Midland, MI) wells in 35 mm culture dishes. Trunk skin and dorsal tail muscle were removed with the aid of an electrolytically sharpened tungsten needle and fine forceps. Then the needle was used to lightly score the meningeal membranes along the dorsal midline of the spinal cord to expose the cell bodies of dorsal and dorsolateral neurons. Embryos were removed from their jelly membranes in recording solution containing TTX and 50 μM *d*-tubocurare to inhibit muscle movement, and the spinal cord was transected with forceps just caudal to the hindbrain. Trunk skin was removed with needle and forceps, and gut tissue was cut away to the ventral edge of the myotomal muscle. Preparations were pinned through the muscle and notochord into a Sylgard well and, in most cases, exposed for 5–10 min to collagenase B (0.1 mg/ml; Boehringer Mannheim, Indianapolis, IN), which facilitated the dissection of dorsal myotomal muscle from the spinal cord. Collagenase-containing solution then was replaced with fresh recording solution. We did not observe any differences in mEPSC properties in collagenase-treated versus untreated preparations.

Electrophysiological recordings. Preparations were visualized at 500× magnification with interference contrast optics on an upright Zeiss microscope and superfused continuously with recording saline (~2 ml/min) in a bath volume maintained at ~0.5 ml. Whole-cell voltage-clamp recordings (Hamill et al., 1981) of spontaneous miniature synaptic currents (mEPSCs) and kainate-evoked whole-cell currents were made with a Dagan 8900 amplifier (Dagan, Minneapolis, MN). Recording pipettes were pulled from 100 μl capillaries (Drummond Scientific, Broomall, PA) with a Flaming/Brown electrode puller (model P-87, Sutter Instruments, Novato, CA) and had 3–5 MΩ resistances when filled with pipette solution. Seals were formed on exposed and clearly visualized cell bodies (10–20 μm diameter) by applying gentle suction to the pipette, followed by a manual suction pulse to achieve whole-cell configuration. All recordings were obtained from neurons positioned in the dorsal quarter of the spinal cord just lateral to Rohon–Beard sensory neurons. These neurons are most likely either dorsolateral commissural or dorsolateral ascending interneurons (Roberts and Clarke, 1982; Clarke and Roberts, 1984; Roberts et al., 1988; Sillar and Roberts, 1988; Sillar and Simmers, 1994). By previous convention (Sillar and Simmers, 1994; Rohrbough and Spitzer, 1996) they are denoted here as dorsolateral interneurons (DLi).

DLi receive excitatory glutamatergic input from Rohon–Beard neurons as well as inhibitory input from other interneurons (Dale, 1995). In initial recordings from mature larvae in standard external saline (see below) containing no added drugs, several classes of spontaneous synaptic currents were observed consistently. The most frequent class of currents reversed near the expected Cl^- equilibrium potential, had monoexponential decay time constants of ~10 msec, and were abolished by 1 μM strychnine, indicating that they were glycinergic mIPSCs. To unambiguously isolate glutamatergic mEPSCs, we made all recordings that were analyzed for this study in the presence of 0.1 μg/ml TTX, 1 μM strychnine, and 50 μM bicuculline to block action potential-evoked synaptic currents and mIPSCs mediated by glycine or GABA, respectively. mEPSCs were recorded at holding potentials between −70 and +60 mV. Series resistance (R_S) estimated from current transients (digitized at 50 kHz) generated by a 10 mV depolarizing step from −70 mV was typically 4–10 MΩ. Because the maximum amplitude of mEPSCs was several hundred picoamps, electronic compensation for R_S was usually not applied. Whole-cell access was monitored at regular intervals during recordings, and data were discarded if R_S was not stable. Whole-cell responses to kainate were evoked by focal pressure application (100–200 msec, ~3 psi) of 500 μM kainic acid in external saline, using a patch pipette positioned 30–40 μM from the cell.

Data acquisition and analysis. Continuous amplified current signals were filtered at 1 kHz and stored on videotape (Neurocorder model DR-390, Neuro Data Instruments, New York, NY). Selected portions were digitized later at 5 kHz by using DMA TL-1 interface hardware and pClamp Fetchex 5.5 software (Axon Instruments, Foster City, CA). mEPSC detection and sorting were performed with analysis software (ACSPLOUF) written and generously provided by Dr. Pierre Vincent (University of California, San Diego), described elsewhere (Vincent and Marty, 1993). Briefly, a user-defined detection window captured current transitions when they exceeded a threshold above baseline within a specified interval of three to four digitized points (0.6–0.8 msec). The detection threshold typically was set at 6–7 pA. Peak amplitude and time-to-peak for each event were determined relative to the preceding portion (2–5 msec) of the window, which was averaged and assigned as baseline. Each detected event was displayed on a computer monitor along with its idealized amplitude and rise time and visually reviewed so that noise, superimposed events, and obvious artifacts could be rejected. In most cases, >100 mEPSCs were collected under control conditions as well as for each pharmacological condition that was assayed, except for AMPA-R antagonists. Cells for which <50 mEPSCs were recorded in control saline (usually embryonic neurons) were excluded from analysis. For recordings in Mg^{2+}-free saline, the set of accepted events for each record then was reviewed and sorted further into several kinetic categories (i.e., fast, dual, slow). The individual events assigned to each category, numbering from between 5 and 10 to several hundred events, were aligned on the rising phase and averaged to generate a mean mEPSC. The rise time, peak amplitude, and decay kinetics of the mean mEPSC reliably reflected the properties of individual mEPSCs and provided a convenient method for illustrating overall amplitude and kinetic properties of mEPSCs during development. Peak amplitudes and decay time constants of mean mEPSCs were measured with Clampfit 6 analysis software (Axon Instruments). For recordings in 1 mM Mg^{2+}, mEPSC kinetic properties were nearly homogeneous, and mean amplitude therefore was determined by averaging the amplitudes of all mEPSCs in the record. In a subset of these recordings, mEPSCs also were divided into fast and dual categories. Dendritic filtering did not appear to contribute significantly to mEPSC variability, because both small- and large-amplitude fast mEPSCs had similar rise times and decay kinetics.

For a subset of recordings (eight embryonic neurons and nine mature neurons) made at −70 mV in 1 mM Mg^{2+}, a modified event-detection protocol was applied to analyze properties of mEPSC bursts, in which successive events were separated by brief intervals. The width of the event detection window was reduced to four digitized points (0.8 msec), with the baseline for each event determined by a single point preceding the threshold crossing. Using these parameters, we reliably detected and measured successive peaks and interpeak intervals as brief as 0.8–1.0 msec. Rare mEPSCs separated by briefer intervals or those with nearly superimposed rising phases were not resolved as distinct events. No correction was made for underestimated peak amplitudes of mEPSCs occurring on the falling phase of the preceding event. However, because fast mEPSC lifetime was <2 msec (~0.4 msec rise times and ~1 msec decay constants), amplitude errors were limited to those events preceded by intervals <2 msec. These mEPSCs represented only a small fraction of all events occurring in bursts, which we arbitrarily defined as mEPSCs separated by <20 msec.

Kainate-evoked whole-cell currents were recorded at potentials from −90 to +60 mV, digitized directly to disk at 1 kHz, and analyzed with pClamp6.

Reversal potential measurements and determination of calcium permeabilities. Estimations of relative Ca^{2+} permeability of AMPA receptors were made by using the Goldman–Hodgkin–Katz equation extended to accommodate divalent cations, with the assumption that Cs^+, K^+, and Na^+ are equally permeant (Mayer and Westbrook, 1987; Gilbertson et al., 1991). Ionic activity estimates rather than concentrations were used for these calculations, using activity coefficients of 0.8 for Cs^+, K^+, and

Na^+ and 0.5 for Ca^{2+} (Jahr and Stevens, 1993). Liquid junction potentials were measured (Neher, 1992) between the pipette and bath solutions for each combination of solutions used in reversal potential experiments and varied between −5 and −9 mV. Corrections for liquid junction potentials and R_S errors were applied to measured reversal potentials.

Solutions and drugs. The standard external recording solution contained (in mM): 125 NaCl, 3 KCl, 2 $CaCl_2$, and 5 HEPES, pH 7.4, as well as TTX (0.1 μg/ml), bicuculline (50 μM), strychnine (1 μM), and *d*-tubocurare (50 μM). $MgCl_2$ (1 mM) was added for recordings in the presence of Mg^{2+}. Glycine (10 μM), a required co-agonist for NMDA-R activation, was included in the external solution in some experiments. Solutions were changed by manually switching a four-way stopcock valve (Hamilton, Reno, NV). The time to exchange the bath was estimated to be 40–60 sec by measuring changes in liquid junction potential with an open recording pipette while exchanging test solutions. To ensure complete exchange during mEPSC recordings, we allowed ~2 min for each solution change. In experiments that used the selective antagonists GYKI 53655 and APV, complete blockade usually was achieved after several minutes of drug perfusion, but much longer periods (>10 min) of washing were necessary for complete or nearly complete reversal, particularly for GYKI (see Fig. 3). It also was difficult to reverse the effects of Mg^{2+}, which blocks NMDA-R in *Xenopus* spinal neurons with a K_D of ~20 μM (Zhang and Auerbach, 1995), even after extensive washing in saline with no added Mg^{2+}. Therefore, once these antagonizing agents had been applied, we avoided making recordings in standard saline from a second cell in the same preparation.

mEPSC reversal potential measurements were made in external salines containing 1 or 20 mM Ca^{2+}. The 1 mM Ca^{2+} solution contained (in mM): 95 NaCl, 3 KCl, 1 $CaCl_2$, 1 $MgCl_2$, 30 *N*-methyl-D-glucamine-Cl (NMG-Cl), 50 μM APV, and 5 HEPES, pH 7.4. In the 20 mM Ca^{2+} solution, NMG-Cl was replaced with 20 mM $CaCl_2$ to maintain an invariant concentration of permeable monovalent cations. $CdCl_2$ (100 μM) was included to reduce current noise at depolarized voltages caused by Ca^{2+} conductances, improving the resolution of mEPSCs near the reversal potential. In cultured spinal neurons 200 μM Cd^{2+} has no detectable effect on NMDA receptor current amplitude and reduces AMPA receptor current by no more than 13% (Gleason and Spitzer, 1998). Kainate reversal potentials were recorded in 0-Na^+ external saline containing (in mM): 95 NMG-Cl, 20 $CaCl_2$, 3 KCl, 1 $MgCl_2$, and 5 HEPES, pH 7.4.

Standard pipette solution contained (in mM): 120 CsCl, 5 EGTA, 2 Mg-ATP, and 10 HEPES, pH 7.4. KCl was substituted for CsCl in the patch solution in some recordings; no differences in mEPSC properties were observed between these two solutions. NaCl, KCl, $MgCl_2$, and $CaCl_2$ were obtained from Fisher Scientific (Tustin, CA) and HEPES from Research Organics (Cleveland, OH). Kainate, CNQX, and APV (2-amino-5-phosphonovaleric acid) were obtained from Research Biochemicals (Natick, MA). GYKI 53655 is a 2,3-benzodiazepine compound that is a highly selective noncompetitive antagonist of AMPA-preferring receptors without effect on kainate-preferring receptors (Donevan and Rogawski, 1993; Zorumski et al., 1993; Paternain et al., 1995). GYKI was a generous gift of Dr. D. Leander (Lilly Research Laboratories, Indianapolis, IN). Other chemicals and drugs were obtained from Sigma (St. Louis, MO).

Statistics. The two-tailed Student's *t* test was used for statistical analysis, and *p* values ≤ 0.05 were taken to be significant. Variability in mEPSC amplitudes recorded in each neuron is reported as SD. All other data, including mean SDs, are reported as mean ± SEM.

RESULTS

Three classes of spontaneous mEPSCs are evident in dorsolateral interneurons of mature larvae in the absence of Mg^{2+}

Whole-cell recordings of spontaneous mEPSCs were made from cell bodies of visually identified neurons in the dorsolateral spinal cord (Fig. 1). These DLi (Sillar and Simmers, 1994; Rohrbough and Spitzer, 1996) are likely either dorsolateral commissural or ascending interneurons (Roberts and Clarke, 1982; Clarke and Roberts, 1984; Sillar and Roberts, 1988).

In mature (5–8 d) larvae three types of mEPSCs, distinguishable by their peak amplitudes and kinetic properties, are observed in most recordings from DLi held at −70 mV in Mg^{2+}-free saline containing 0.1 μg/ml TTX (Fig. 2*A,B*). These mEPSCs are categorized as "fast," "slow," or "dual" (dual component). Dual mEPSCs are most common, constituting 71 ± 2% of all mEPSCs (range, 62–82%; $n = 16$; Table 1). Dual mEPSCs are composed of an initial fast component with a rapid rise time (mean rise time <300 μsec) and decay time constant of ~1 msec, followed by a smaller and much slower component of variable duration, in which single channel current transitions of −4 to −5 pA occasionally can be resolved (Fig. 2*B*). A minority (21 ± 2%; range, 10–38%) of mEPSCs having only a fast current component also is observed in nearly all (15 of 16) cells. Fast mEPSCs and the fast component of dual mEPSCs have mean peak amplitudes of −28 ± 2 and −34 ± 3 pA, respectively, and are kinetically indistinguishable (Fig. 2*B,C*, Table 1). mEPSC rise times and peak amplitudes exhibit only a slight, positive correlation (data not shown), indicating that they are not influenced significantly by electrotonic filtering. Both fast and dual mEPSCs also are recorded at strongly depolarized potentials (+60 mV; Fig. 2*C*). In addition, a third class of slow, noisy mEPSCs resembling the slow component of dual mEPSCs is observed with a low incidence (8 ± 2%; range, 0–23%; $n = 16$) in most records (Fig. 2*B1*). Slow mEPSCs are initiated by the approximately synchronous opening of two to three individual channels of −4 to −5 pA amplitude. In addition, individual single channel openings by the same class of receptors (see below) can be resolved in many recordings. Because it was impossible to discern whether this channel activity results from synaptic receptor activation or from the diffusion of transmitter to nonsynaptic receptors, it is not included in mEPSC analyses.

To better quantify the properties of these three populations of mEPSCs at mature larval synapses, we constructed mean mEPSCs by averaging dual, fast, and slow mEPSCs recorded from each neuron (Fig. 2*B2,C2*). Mean dual mEPSCs in most cases are well fit by two exponentials, having fast time constants of 1.1 ± 0.1 msec ($n = 16$). The slow time constant of dual mEPSCs is 10–50 times longer at −70 mV (mean, 26.8 ± 5.4 msec; $n = 16$; Table 1), and is prolonged two- to threefold by depolarization to +60 mV (Fig. 2*B,C*; $n = 4$). Although the slow current component of dual mEPSCs averages only −8 to −10 pA

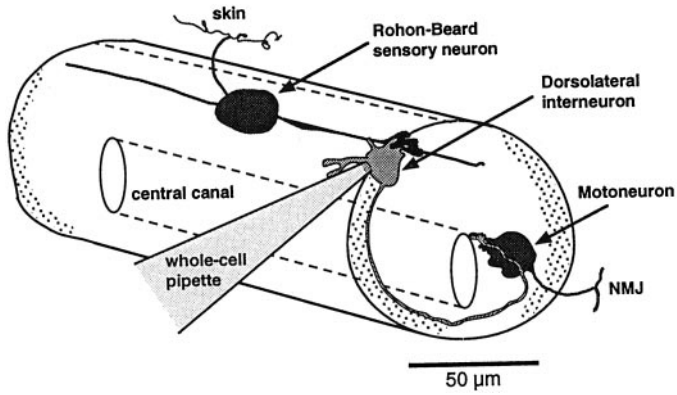

Figure 1. Excitatory synapses on dorsolateral interneurons (DLi) are examined in intact *Xenopus* embryonic and larval spinal cords. A schematic representation of neurons in the early larval spinal cord is shown. Glutamatergic mEPSCs described in this study originate from Rohon–Beard cells. The DLi also receive inhibitory input from other interneurons (data not shown) and make excitatory connections onto motoneurons. Whole-cell recordings were made between developmental stages 31 (39 hr after fertilization) and 48 (7–8 d) from interneurons identified by the superficial location of their cell bodies in the dorsolateral spinal cord.

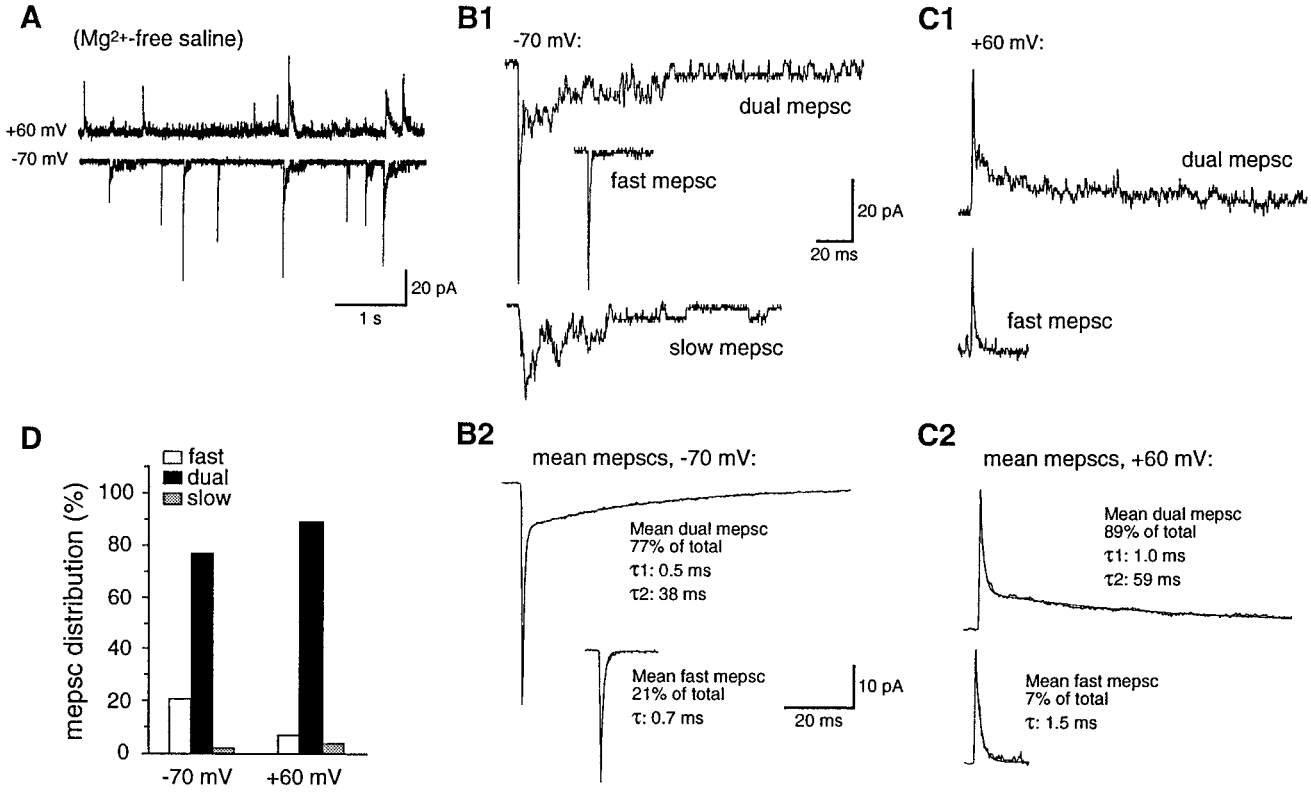

Figure 2. mEPSCs recorded from mature excitatory synapses are predominantly dual component in Mg^{2+}-free saline. *A*, Continuous traces of mEPSCs recorded at −70 mV (*bottom trace*) and +60 mV (*top trace*). All recordings in this and subsequent figures were made in the presence of TTX (0.1 μg/ml), strychnine (1 μM), and bicuculline (50 μM) to block action potentials and mIPSCs. *B, C*, Examples of dual-component (dual mEPSCs), fast, and slow mEPSCs recorded at −70 mV (*B1*) and dual and fast mEPSCs recorded at +60 mV (*C1*). Dual mEPSCs, consisting of a fast initial current component followed by a variable slow decay, predominated at both potentials. *B2, C2*, Mean dual-component ($n = 113$, −70 mV; $n = 49$, +60 mV) and fast mEPSCs ($n = 34$, −70 mV; $n = 3$, +60 mV); slow mEPSCs were too infrequent to construct an average. Single-exponential (fast mEPSCs) and double-exponential (dual mEPSCs) fits are superimposed on the mean mEPSC traces. *D*, Distribution of fast, dual-component, and slow mEPSCs at both potentials. All data are from a single DLi in a 6 d larva.

in amplitude, it constitutes ~90% of the current area of the mean dual mEPSC. Mean fast mEPSCs are fit adequately in most cases by a single time constant (Fig. 2*B,C*) that does not differ significantly at −70 mV (0.8 ± 0.1 msec; $n = 16$) from the fast time constant of dual mEPSCs (Table 1). Because slow mEPSCs occur rarely and vary substantially in duration at −70 mV, their kinetic properties were not quantified.

mEPSCs at mature synapses are mediated by both AMPA-R and NMDA-R

To determine which glutamate receptor subtypes underlie mEPSCs at DLi synapses in mature larvae, we studied the effects of specific AMPA-R and NMDA-R antagonists. GYKI 53655 (25–50 μM), a highly selective noncompetitive antagonist of AMPA-R (Donevan and Rogawski, 1993; Zorumski et al., 1993; Paternain et al., 1995), completely and selectively abolishes both fast mEPSCs and the fast component of dual mEPSCs after several minutes of exposure, while sparing the slow current component (Fig. 3*A,B*; $n = 6$). In the presence of GYKI, the addition of 1 mM Mg^{2+}, a voltage-dependent blocker of NMDA-R channels, abolishes the remaining slow mEPSCs at −70 mV, revealing occasional bursts of single channel openings. These channel events have an estimated conductance of ~50 pS (assuming a reversal potential of 0 mV; $n = 3$), which is close to the expected size for NMDA-R channels undergoing periodic relief of Mg^{2+} blockade (Zhang and Auerbach, 1995). At strongly depolarized potentials (+30 to +60 mV) expected to relieve the Mg^{2+} blockade of NMDA-R, slow mEPSCs are revealed ($n = 3$) with decay constants several-fold longer than at −70 mV (Fig. 3*B*; also 2*B,C*), demonstrating a positive effect of voltage on NMDA-R synaptic current decay similar to that reported previously (Hestrin, 1992).

APV (50–100 μM), a specific NMDA-R antagonist, selectively abolishes the slow component of mEPSCs as well as background single NMDA-R channel openings within 2–3 min exposure ($n = 5$). The mean mEPSC remaining in APV is indistinguishable from the control fast mEPSC at both negative and positive potentials (Fig. 3*C,D*). These results demonstrate that the fast and slow mEPSC components are mediated by AMPA-R and NMDA-R, respectively.

Glycine is a required co-agonist for NMDA-R activation (Johnson and Ascher, 1987). The addition of 10 μM glycine to the external saline in recordings from mature DLi does not change the distribution of mEPSCs significantly ($n = 4$; data not shown), suggesting that in control recordings glycine is present at endogenous levels sufficient to permit NMDA-R activation. Larval DLi also receive strong glycinergic inhibitory synaptic input (Dale, 1995). In recordings from mature larvae in drug-free standard saline (data not shown), we consistently observed frequent mIPSCs that were abolished after the addition of 1 μM strychnine; thus endogenous glycine may be supplied by spontaneous release at nearby inhibitory synapses.

Table 1. Developmental changes in amplitudes and kinetics of mEPSCs recorded at −70 mV in Mg^{2+}-free and 1 mM Mg^{2+}-containing salines

	Embryonic (39–40 hr)	Early larval (54 hr)	Mature (5–8 d)
I. Mg^{2+}-free saline			
a. Peak amplitudes (pA)			
fast mEPSCs	−55 ± 6 (5)	−46 ± 9 (6)	−28 ± 2 (16)
dual mEPSCs	−72 ± 10	−56 ± 11	−34 ± 3
b. Decay time constants (ms)			
fast mEPSC τ	1.1 ± 0.2 (5)	1.2 ± 0.1 (6)	1.1 ± 0.1 (16)
dual mEPSC fast τ	0.9 ± 0.1	1.2 ± 0.2	0.8 ± 0.1
dual mEPSC slow τ	8.2 ± 2.0	21.8 ± 7.6	26.8 ± 5.4
c. Incidence of dual mEPSCs	32 ± 5% (5)	40 ± 3% (6)	71 ± 2% (16)
II. 1 mM Mg^{2+} saline			
a. Peak amplitudes (pA)			
mean mEPSC*	−74 ± 7 (17)	—	−30 ± 2 (13)
b. Decay time constants (ms)			
fast mEPSC τ**	0.7 ± 0.7 (6)	—	1.0 ± 0.2 (4)
dual mEPSC fast τ**	0.6 ± 0.0	—	0.7 ± 0.1
dual mEPSC slow τ**	5.5 ± 0.9	—	4.4 ± 0.3
c. Incidence of dual mEPSCs	7 ± 1% (6)	—	14 ± 3% (4)

mEPSC amplitude, decay time constants, and incidence during development. I. mEPSC properties in Mg^{2+}-free external saline at embryonic (39–40 hr), early larval (54 hr), and mature larval (5–8 d) developmental stages. II. mEPSC properties in 1 mM Mg^{2+}-containing external saline at embryonic and mature stages. Mean mEPSC peak amplitude in 1 mM Mg^{2+} (a; *) was determined in 17 embryonic and 13 mature cells by averaging peak amplitudes of all mEPSCs in each record (see Materials and Methods). In six embryonic and four mature recordings, mEPSCs were subcategorized further as fast or dual (b; **) to measure decay time constants of fast and dual mEPSCs and incidence of dual mEPSCs (c). Number of experiments (n) in each section is indicated in parentheses; n for the first value applies to those immediately beneath.

mEPSCs at embryonic synapses are mediated predominantly by AMPA-R

To study the involvement of AMPA-R and NMDA-R at excitatory synapses during their development, we examined the pharmacological and kinetic properties of mEPSCs in DLi in stage 31/32 embryos (39–40 hr). This stage is ~13 hr after reflex movements are first detectable, but it precedes hatching and the free-swimming larval stage by 15 hr (Nieuwkoop and Faber, 1967). mEPSC frequency at these early stages of development is highly variable, and in some cells too few events were recorded for statistically significant analysis. However, at −70 mV in Mg^{2+}-free saline, all neurons in which activity is recorded exhibit both fast mEPSCs with rapid rise times and decays and dual mEPSCs with slower decay components (Fig. 4; $n = 5$). The fast and slow components of embryonic mEPSCs are blocked selectively by GYKI (Fig. 4*A,B*; $n = 4$) and Mg^{2+} ($n = 3$) or APV ($n = 2$), respectively (Fig. 4*C,D*), indicating that, as at mature synapses, they are mediated by AMPA-R and NMDA-R.

Embryonic mEPSC distribution and peak amplitudes in Mg^{2+}-free saline differ markedly from those at mature synapses, however (Fig. 5, Table 1). At −70 mV the majority (66 ± 6%; range, 47–78%; $n = 5$) of embryonic mEPSCs is exclusively fast, with peak amplitudes twofold larger than mature fast mEPSCs. Dual mEPSCs occur more rarely (32 ± 5%; range, 21–50%; $n = 5$) and also have peak amplitudes over twofold larger than in mature larvae. The rise times and decay kinetics of fast mEPSC current components are indistinguishable from those at mature stages. However, the slow NMDA-R-mediated component of embryonic dual mEPSCs is less prominent and has a significantly faster decay constant (8.2 ± 2.0 msec; $n = 5$) than at mature synapses. Single channel activity resembling NMDA-R channel openings is also sometimes present, but slow mEPSCs are observed only rarely (3 ± 2%; range, 1–9%; $n = 5$).

The predominance of fast mEPSCs at embryonic excitatory spinal synapses suggests that they differ in two possible respects from mature larval synapses: (1) the majority of embryonic synapses expresses only AMPA-R; or (2) NMDA-R are present, but most are nonfunctional or blocked, even in the absence of added Mg^{2+}. The large, predominantly fast AMPA-R-mediated mEPSCs present at immature synapses gradually undergo a developmental transition to smaller dual-component mEPSCs mediated by both AMPA-R and NMDA-R in Mg^{2+}-free saline.

At an early larval stage (54 hr), mEPSC pharmacology is identical to that at embryonic and mature stages ($n = 6$; data not shown). Mean mEPSC amplitudes and the distribution of dual and fast mEPSCs at this stage are intermediate between embryonic and mature values ($n = 6$; Fig. 5, Table 1), indicating that these properties are changing gradually during development. By mature larval stages, AMPA-R and NMDA-R are colocalized at most synapses, evidenced by the 71% incidence of dual-component mEPSCs (Fig. 5). Depolarization to +60 mV slightly increases the incidence of dual and slow mEPSCs (see Fig. 2*D*; $n = 4$), probably attributable to relief of a small amount of residual Mg^{2+} block of NMDA-R at −70 mV, and prolongs the decay constant of the NMDA-R component by two- to threefold. However, as noted above, fast mEPSCs are still observed even at +60 mV. These results indicate that both AMPA-R and NMDA-R are colocalized at ≥70% of mature excitatory synapses, whereas most of the remaining synapses express only AMPA-R.

Early excitatory transmission at these spinal synapses thus is mediated principally by AMPA-R rather than by NMDA-R. This finding contrasts with several studies in mammalian hippocampus (Durand et al., 1996; Liao and Malinow, 1996), sensory cortex (Crair and Malenka, 1995; Isaac et al., 1997) and spinal motoneurons (Ziskind-Conhaim, 1990), and in *Xenopus* optic tectum (Wu

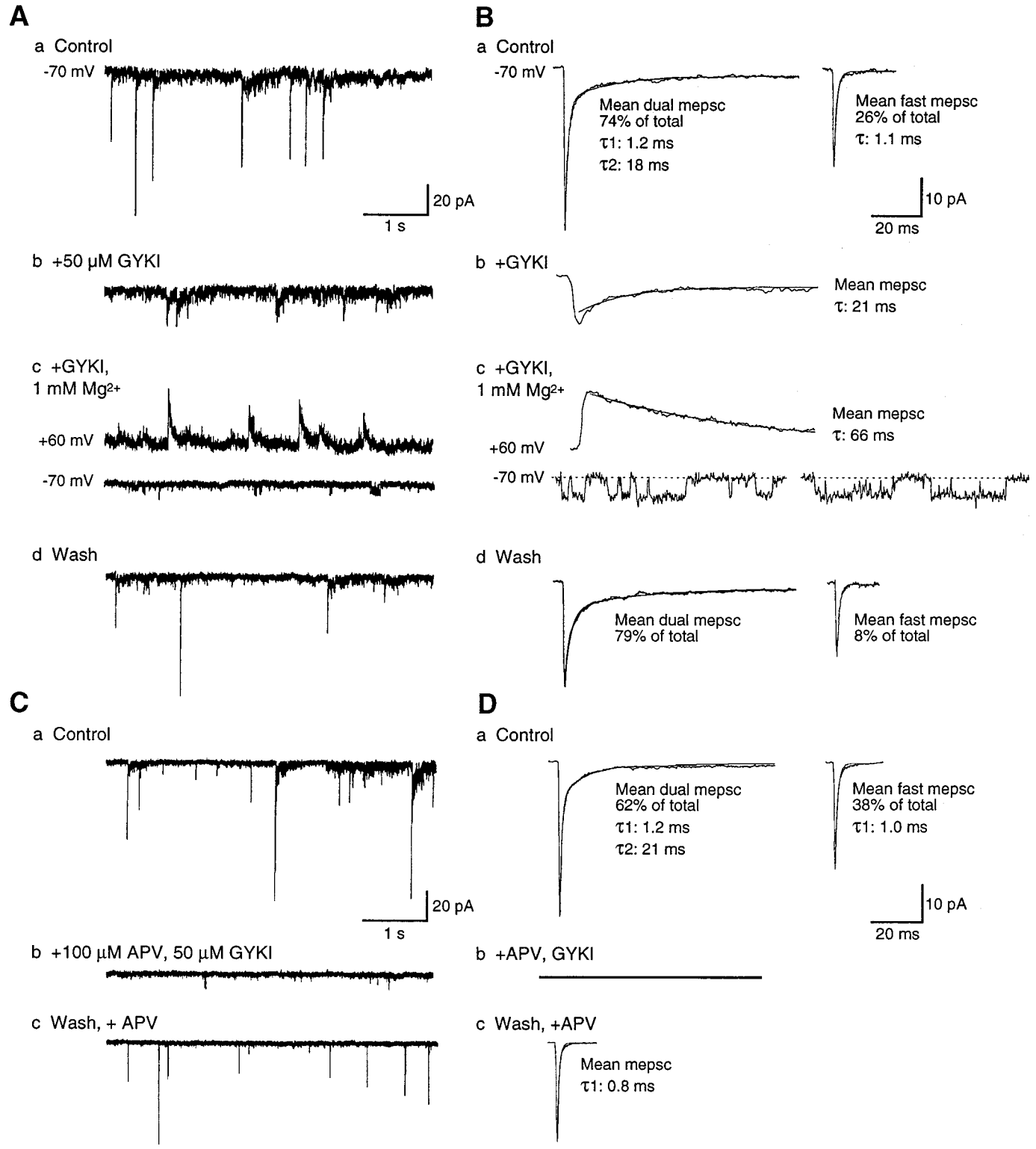

Figure 3. mEPSCs at mature excitatory spinal synapses are mediated by both AMPA-R and NMDA-R. *A, B*, GYKI and Mg^{2+} selectively block the fast and slow mEPSC components, respectively. *A*, Continuous traces of mEPSCs recorded at −70 or +60 mV, as indicated. *B*, Mean mEPSCs are shown for each corresponding segment of the recording. *a*, Dual-component mEPSCs predominate in control 0-Mg^{2+} saline. *b*, GYKI blocks fast mEPSCs and the fast component of dual mEPSCs; the mean mEPSC has a slow decay constant comparable to the slow component of the mean dual mEPSC in *a*. *c*, In the continued presence of GYKI the addition of Mg^{2+} blocks all mEPSCs at −70 mV (*lower trace*), although occasional single channel openings of 4–5 pA are observed that may be attributable to synaptic NMDA-R. At depolarized potentials (+60 mV; *upper trace*), outward mEPSCs with prolonged decay constants are evident. These results indicate that fast mEPSC components are mediated by AMPA-R, and the slow component is mediated by NMDA-R. *d*, Both dual-component and fast mEPSCs are recorded after >8 min washout of GYKI and Mg^{2+}. *C, D*, APV selectively abolishes the slow mEPSC component. Traces (*C*) and averaged mEPSCs (*D*) at −70 mV are illustrated as in *A* and *B*. *a*, Dual-component and fast mEPSCs recorded in control 0-Mg^{2+} saline. *b*, In the presence of APV and GYKI all mEPSCs are abolished. *c*, After the washout of GYKI in (*Figure legend continues*)

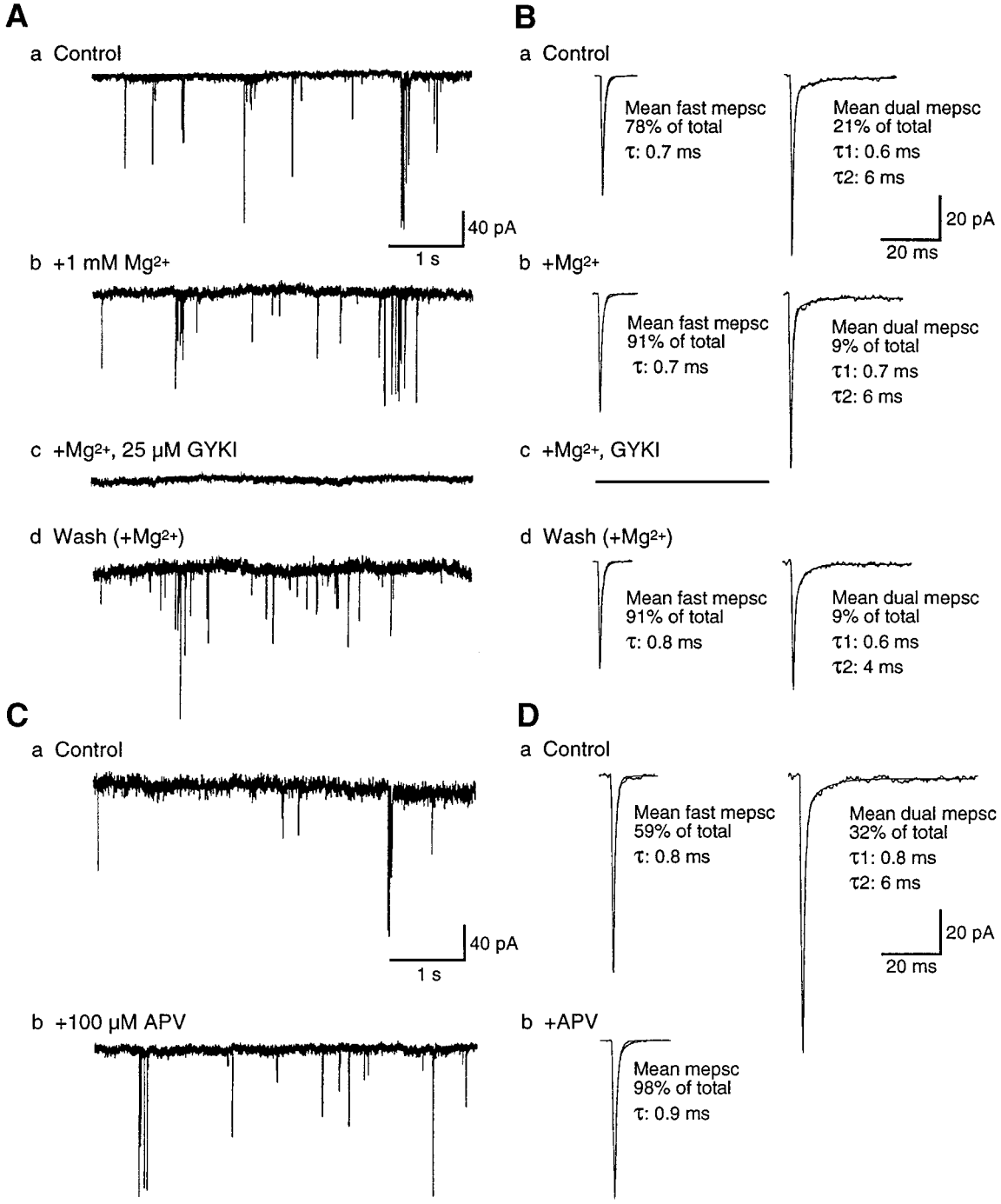

Figure 4. mEPSCs at embryonic excitatory spinal synapses are mediated primarily by AMPA-R. *A, B*, GYKI and Mg^{2+} selectively block the fast and slow embryonic mEPSC components, respectively. *A*, Continuous traces of mEPSCs recorded at −70 mV. *B*, Mean mEPSCs for each corresponding segment of the recording. *a*, Fast mEPSCs predominate in control 0-Mg^{2+} saline, and the slow component of dual mEPSCs is proportionately smaller and briefer than in mature mEPSCs (see Fig. 3*B*). *b*, The addition of Mg^{2+} reduces the incidence of dual mEPSCs to <10%. *c*, All mEPSCs are abolished in the presence of Mg^{2+}plus GYKI. *d*, After the washout of GYKI, fast mEPSCs again predominate. *C, D*, APV reveals a minor NMDA-R-mediated component in embryonic dual mEPSCs. Continuous traces (*C*) and averaged mEPSCs (*D*) at −70 mV are illustrated as in *A* and *B*. *a*, The majority of mEPSCs recorded in control 0-Mg^{2+} saline are fast. *b*, In the presence of APV only fast mEPSCs remain, which are indistinguishable from the fast control mEPSCs. *A, B* and *C, D* were recorded from two cells in different stage 31/32 (39–40 hr) embryos. Mean mEPSCs are averages of ≥49 events (fast) and ≥18 events (dual).

←

the continued presence of APV, only fast mEPSCs are observed, which are indistinguishable from fast mEPSCs observed in control saline. *A, B* and *C, D* were recorded from two cells in different mature 7 d larvae; the recording in *A* and *B* was made in the presence of 10 μM glycine, which did not change the distributions of mEPSCs significantly ($n = 4$). Mean fast mEPSCs are averages of 7–21 events; other mean mEPSCs are averages of >50 events.

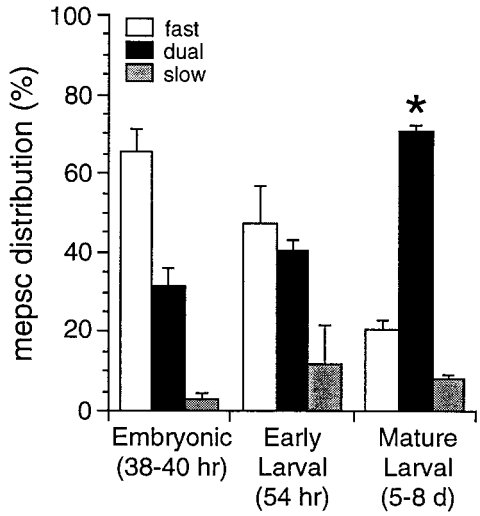

Figure 5. The distribution of different classes of mEPSCs changes during embryonic and larval development. The mean percentages ± SEM of fast, dual, and slow mEPSCs recorded at −70 mV in Mg^{2+}-free external saline are plotted for three developmental stages. The incidence of dual, AMPA-R- and NMDA-R-mediated, mEPSCs increases to >70% at mature synapses, and the incidence of fast AMPA-R-mediated mEPSC decreases. The percentage of dual mEPSCs in mature larvae (*asterisk*; 71 ± 2%; $n = 12$) is significantly greater than the values at both embryonic (38–40 hr; $n = 5$) and larval stages (54 hr; $n = 6$).

et al., 1996), where NMDA-R-mediated synaptic currents precede AMPA-R-mediated synaptic currents. Our finding is in agreement, however, with a recent developmental study of cultured *Xenopus* embryonic spinal neurons showing that AMPA-R expression precedes NMDA-R expression and that AMPA-evoked currents are 10-fold larger than NMDA-evoked currents at 1 d in culture (~40 hr of embryonic development) (Gleason and Spitzer, 1998).

mEPSCs at both embryonic and mature synapses are mediated essentially by AMPA-R in the presence of Mg^{2+}

The addition of 1 mM Mg^{2+} to the external saline blocks nearly all of the NMDA-R-mediated synaptic current at −70 mV at embryonic as well as mature larval synapses, converting most dual mEPSCs to fast mEPSCs and eliminating slow mEPSCs. As a result, ~90% of both mature and embryonic mEPSCs in the presence of Mg^{2+} are exclusively fast, and the slow decay time constant in the few remaining mature dual mEPSCs is shortened significantly to ~5 msec (Table 1). Dual mEPSCs with prolonged slow current components are revealed only at strongly depolarized potentials (+30 to +60 mV; $n = 4$). At negative potentials (−30 to −70 mV) the mean mEPSC in Mg^{2+} is kinetically similar to the fast mEPSCs described above, with a decay constant of ~1 msec. Consistent with earlier results, embryonic mEPSCs in Mg^{2+} are over twice as large as mature mEPSCs (Table 1). Thus, over a broad range of negative potentials, synaptic NMDA-R are functionally blocked in the presence of a physiological Mg^{2+} concentration. Under most normal conditions the excitatory current at DLi synapses therefore must be mediated almost entirely by AMPA-R, even at mature synapses that express NMDA-R. This finding further strengthens the conclusion that initial excitatory transmission in the embryonic spinal cord is mediated mainly by AMPA-R.

AMPA-R are permeable to Ca^{2+}

AMPA-R in cultured embryonic *Xenopus* spinal neurons are permeable to Ca^{2+} (Gleason and Spitzer, 1998). Because transmission at excitatory DLi synapses is mediated predominantly by AMPA-R, we investigated the Ca^{2+} permeability of these receptors. AMPA-R at embryonic synapses are also permeable to Ca^{2+}. The mEPSC reversal potential in the presence of APV and Mg^{2+} is shifted in the positive direction by 10 ± 1 mV ($n = 5$) when external Ca^{2+} is raised from 1 to 20 mM (Fig. 6*A*). Using the Goldman–Hodgkin–Katz equation, we calculate a relative Ca^{2+} permeability ($P_{Ca}/P_{monocation}$) of 1.7 ± 0.3 (range, 1.0 to 2.5; $n = 6$) for embryonic synaptic AMPA-R, a value similar to that found for AMPA-R (relative P_{Ca} of 1.9) in cultured spinal neurons (Gleason and Spitzer, 1998).

As a second, independent test for AMPA-R Ca^{2+} permeability, we recorded whole-cell responses to puffer-applied 500 μM kainate (KA) in 0-Na^+, 20 mM Ca^{2+} saline (Gu et al., 1996; Jia et al., 1996), which likely activates both synaptic and nonsynaptic AMPA-R populations. KA reversal potentials for embryonic and mature larval DLi are −22 ± 4 mV ($n = 4$) and −30 ± 1 mV ($n = 3$), respectively (Fig. 6*B*), indicating significant Ca^{2+} permeabilities for AMPA-R in both embryonic and mature neurons. For embryonic AMPA-R, relative P_{Ca} values determined from KA reversal potentials (1.5 ± 0.1; $n = 4$) and mEPSC reversal potential experiments do not differ significantly, suggesting that Ca^{2+} permeabilities of both synaptic and nonsynaptic receptors are similar. For mature AMPA-R, relative P_{Ca} determined from KA reversal potentials is 1.0 ± 0.1 ($n = 3$). This value is significantly less than that for embryonic receptors, but nevertheless it indicates a substantial P_{Ca} for AMPA-R during the period of development that was studied. The Ca^{2+} permeability of these AMPA-R raises the possibility that, in addition to mediating excitatory transmission, they allow Ca^{2+} influx from the earliest stages of synaptic activity, which regulates aspects of neuronal maturation and synaptic plasticity.

Developmental changes in presynaptic activity patterns and mEPSC amplitude distributions

Spontaneous activity patterns and amplitudes of AMPA-R-mediated mEPSCs in 1 mM Mg^{2+}-containing saline are strikingly different at embryonic and mature larval synapses (Figs. 7, 8). At embryonic synapses a component of spontaneous transmitter release occurs in a nonrandom manner, with a disproportionate number of mEPSCs occurring in bursts with a high incidence of activity, interspersed with periods of much lower frequency (Figs. 7*A*, 9*B*). Bursts vary from pairs of mEPSCs to over a dozen closely spaced events and are observed in all embryonic recordings. They appear to result from brief episodes of heightened release probability at individual presynaptic inputs, because they occur even when overall mEPSC frequency is low (<1 Hz). The average embryonic mEPSC frequency (2.1 ± 0.6 Hz; $n = 17$) in the presence of these bursts is not significantly less than that in mature neurons (3.0 ± 0.9 Hz; $n = 13$).

To assay bursting behavior, we measured intervals between mEPSCs. The distribution of inter-mEPSC intervals (IMIs) is markedly different between embryonic and mature synapses (Fig. 7*B–D*). All embryonic IMI distributions exhibit a prominent component of brief intervals (<20 msec; Figs. 7*C*, 9*A,B*) regardless of overall mEPSC frequency (range, 0.7–9.9 Hz; $n = 8$). By contrast, at mature synapses with comparable frequencies (0.7–13.5 Hz; $n = 9$), brief intervals (<20 msec) are rare, and mature IMI histograms have approximately single-exponential distribu-

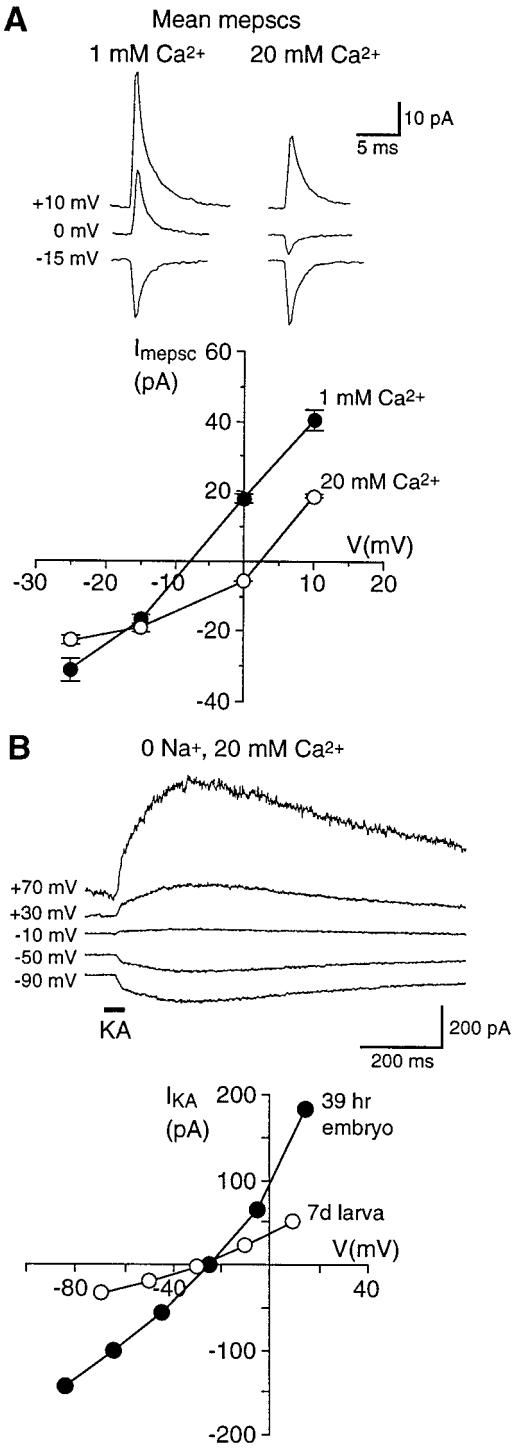

Figure 6. Embryonic synaptic AMPA-R and the total AMPA-R population in both embryonic and mature larval DLi are Ca^{2+}-permeable. *A*, *Top*, Mean AMPA-R-mediated mEPSCs recorded in 1 and 20 mM external Ca^{2+} at three holding potentials from a DLi in a stage 31 (39 hr) embryo. Mg^{2+} (1 mM) and APV (50 μM) were present to isolate AMPA-R. Note that the mean mEPSCs at 0 mV have opposite polarity at the two Ca^{2+} concentrations. *A*, *Bottom*, mEPSC *I–V* relations in 1 and 20 mM Ca^{2+} for the same cell. The mEPSC reversal potential (determined by interpolation) in 20 mM Ca^{2+} is shifted by +10.5 mV, indicating a significant Ca^{2+} permeability for synaptic AMPA-R (estimated P_{Ca} of 1.8 relative to monovalent cations). *B*, Whole-cell responses to kainate (*KA*) in 0-Na^+, 20 mM Ca^{2+} external saline support the conclusion that the AMPA-R population (synaptic plus nonsynaptic) is permeable to Ca^{2+}. *B*, *Top*, Currents evoked by 500 μM KA focally applied with a pressure pipette (*horizontal bar*) in 0-Na^+, 20 mM Ca^{2+} saline to a DLi in a stage 31 embryo. *B, Bottom*, The KA *I–V* in 0-Na^+, 20 mM Ca^{2+} is shown for the same embryonic neuron (*filled symbols*); the KA reversal potential is −22 mV, and the estimated relative P_{Ca} for AMPA-R is 1.5. *Open symbols* show the KA *I–V* in 0-Na^+, 20 mM Ca^{2+} for a DLi in a mature (7 d) larva; the reversal potential is −30 mV, and estimated relative P_{Ca} is 1.0.

tions consistent with the random occurrence of mEPSCs (Fig. 7*D*).

In addition, both mEPSC mean amplitude and variability are significantly greater at embryonic synapses (Figs. 7*C,D*, 8). Mature mEPSCs have amplitude distributions skewed toward larger values, with mean amplitudes of −30 ± 2 pA and SDs of 20 ± 2 pA (n = 13). Embryonic mEPSCs have 2.5-fold larger mean amplitudes (−74 ± 7 pA) and SDs (51 ± 5 pA; n = 17). Interestingly, embryonic synapses appear to fall into "low" and "high" subgroups on the basis of mEPSC mean amplitude and variability, although both groups have significantly greater values than those of mature synapses (Fig. 8*A–C*). The embryonic "low" group has a mean mEPSC amplitude of −53 ± 1 pA and broadly skewed amplitude distributions (SD, 38 ± 2 pA; n = 10) that usually have several wide peaks (Fig. 8*B*). The embryonic "high" group has significantly larger amplitudes (−104 ± 10 pA) and a much wider range in amplitude from cell to cell (Fig. 8*A,B*). mEPSC amplitude distributions for this latter group of neurons are broader (SD, 70 ± 7 pA; n = 7) and occasionally lack a predominant peak (Figs. 7*C*, 8*B*). Mean mEPSC amplitudes and SDs are strongly correlated during development as well as within each age group, suggesting a developmental reduction and refinement in both mEPSC amplitude and variability (Fig. 8*B*). However, the coefficient of variability (CV) does not change significantly and remains surprisingly large (~0.65) even in mature larvae (Fig. 8*C*).

The larger amplitude and variability of mEPSCs at embryonic spinal synapses could be attributable to both pre- or postsynaptic factors thought to contribute to large synaptic current variability at other CNS synapses (Bekkers et al., 1990; Bekkers and Stevens, 1995; Frerking et al., 1995; Nusser et al., 1997; Wall and Usowicz, 1998). One possibility is that the simultaneous fusion of multiple transmitter vesicles occurs with a greater probability at embryonic presynaptic boutons, possibly as a result of spontaneous Ca^{2+} influx at boutons with multiple release sites (Bennett et al., 1995; Frerking et al., 1997). This would be expected to generate broad mEPSC amplitude distributions with multiple peaks, as we observed for all 17 embryonic neurons that were analyzed. However, peak number differs greatly among different distributions and peak intervals are highly inconsistent, thus providing no clear evidence for quantal modes of release (Figs. 7*C*, 8*B*, 9*C*), and inflections or notches on the rising phase of large mEPSCs indicative of multivesicular events (Wall and Usowicz, 1998) are rare.

If large mEPSC amplitudes are generated by a Ca^{2+}-dependent multiquantal release mechanism, then reducing the probability of spontaneous release should result in a decrease of both mEPSC variability and mean amplitude (Frerking et al., 1997; Wall and Usowicz, 1998). To test this possibility directly, we recorded embryonic mEPSCs in both normal 2 mM Ca^{2+} and in saline without added Ca^{2+} (0-Ca^{2+} saline). mEPSC frequency is greatly reduced (18 ± 4% of control; n = 4) in 0-Ca^{2+} saline, as

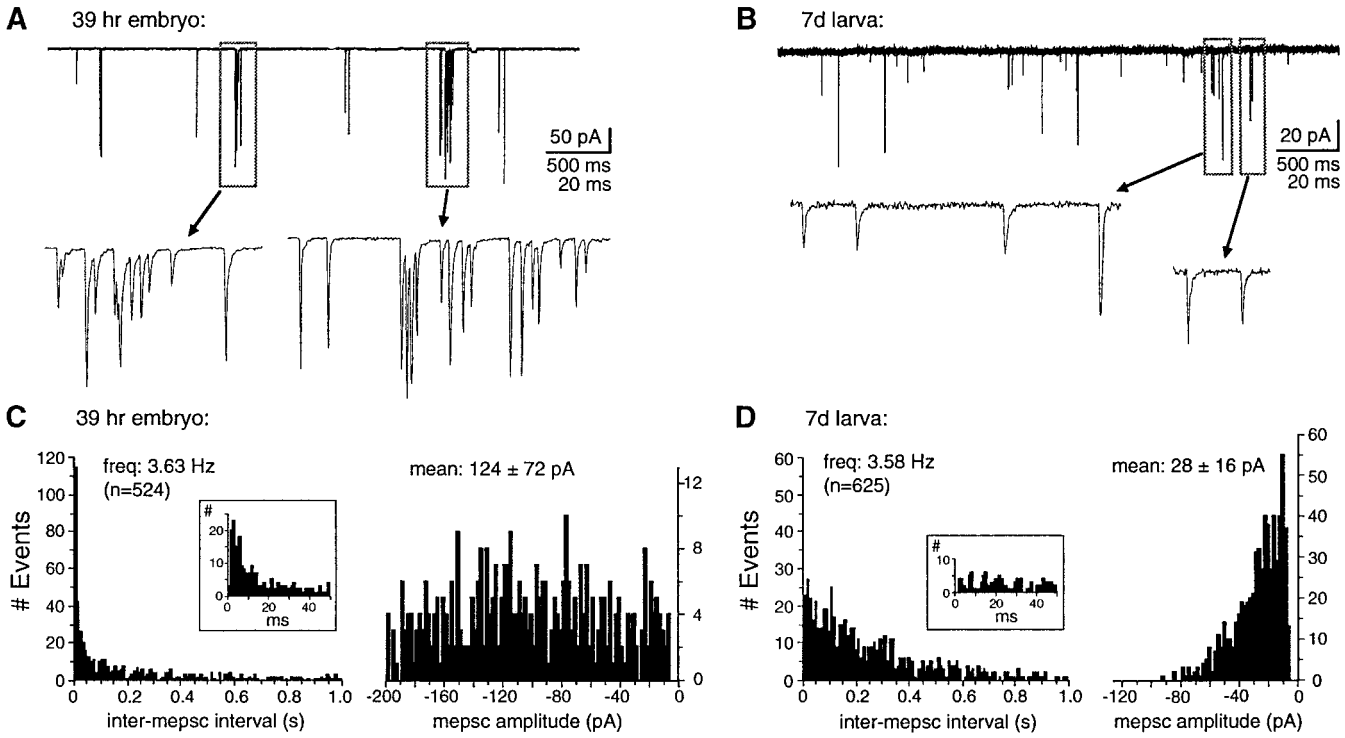

Figure 7. AMPA-R-mediated mEPSCs at embryonic synapses occur in spontaneous bursts and have large amplitudes, both of which are absent at mature synapses. *A, B*, Continuous records (*top traces*) of mEPSCs recorded at −70 mV in 1 mM Mg^{2+} from an embryonic neuron (*A*) and a mature neuron (*B*). Note the difference in amplitude scales. Portions of the continuous traces contained in the *boxed regions* are shown on an expanded time scale (*bottom set* of *traces*). Many mEPSCs at embryonic synapses occur in bursts separated by brief intervals (*A, bottom trace*) even when the overall frequency is low, whereas at mature synapses (*B, bottom trace*) such bursts are absent. *C*, *D*, Inter-mEPSC interval (IMI) distributions (*left panels*) and mEPSC amplitude distributions (*right panels*) for the cells illustrated in *A* and *B*. The proportion of brief IMIs (1–20 msec durations) is markedly greater at the embryonic synapse (*C*) than at the mature synapse (*D*) because of events occurring in bursts, although both cells had the same overall mEPSC frequency; note the different scale of ordinates. *Insets* show distributions of IMIs <50 msec in each cell in greater detail. All embryonic neurons had disproportionately greater numbers of brief IMIs. Embryonic mEPSCs have significantly greater amplitudes and variability than mature mEPSCs. Values *above* IMI distributions are overall frequency and number of events; values *above* amplitude distributions are mean amplitude ± SD.

expected, but mEPSC mean amplitude (99 ± 10% of control) and variability (96 ± 8% of control) are not significantly different from those in 2 mM Ca^{2+} (Fig. 9*C*). These parameters are thus mainly Ca^{2+}-independent and likely derive from factors other than multiquantal release, such as differences in quantal transmitter content (Frerking et al., 1995), synaptic transmitter concentration (Kullmann and Asztely, 1998), and AMPA-R number or availability at different release sites (Walmsley, 1995; Nusser et al., 1997; Walmsley et al., 1998).

In contrast, spontaneous multi-mEPSC bursts are eliminated in 0-Ca^{2+} saline, except for rare doublets (Fig. 9*C*; $n = 4$). This result suggests that the bursts of mEPSCs observed at all embryonic synapses are triggered by spontaneous presynaptic Ca^{2+} entry, resulting in episodes of unsynchronized multiquantal release over a period of several milliseconds to tens of milliseconds. The mechanism generating bursts at embryonic synapses is thus distinct from that underlying larger mEPSC amplitude and variability. Bursts are equally prominent in embryonic neurons in the "low" group, which have smaller mEPSC amplitudes and variability (Fig. 9*A,C*). Moreover, for all of the neurons that were analyzed, the mean amplitude of mEPSCs occurring within high-frequency bursts (<20 msec IMI) does not differ significantly from that of mEPSCs occurring outside of bursts (Fig. 9*B*). At embryonic synapses in particular, large mEPSC amplitudes coupled with the spontaneous bursting of presynaptic transmitter release underscore the possibility that AMPA-R are used as an important source of spontaneous postsynaptic Ca^{2+} entry.

DISCUSSION

Early AMPA-R expression and later colocalization of NMDA-R and AMPA-R at excitatory spinal synapses

mEPSCs at embryonic *Xenopus* DLi spinal synapses are already dominated by fast, large-amplitude AMPA-R currents in Mg^{2+}-free saline within 13 hr after reflex movements begin. Previously, intracellular mEPSP recordings from DLi in newly hatched (54 hr) larvae suggested that non-NMDA-R and NMDA-R were primarily segregated at different postsynaptic sites (Sillar and Roberts, 1991). In contrast, we show that NMDA-R and AMPA-R are colocalized progressively to >70% of individual synapses by mature larval stages, producing distinct mEPSC components similar to those observed at other mature central synapses (Bekkers and Stevens, 1989; Hori and Endo, 1994; Isaacson and Walmsley, 1995; Wu et al., 1996; O'Brien et al., 1997). In parallel, AMPA-R mEPSC amplitudes decrease and NMDA-R mEPSC decay constants lengthen, increasing the relative NMDA-R contribution to mature synaptic currents. However, mEPSCs throughout development are predominantly AMPA-R-mediated under normal physiological conditions (+Mg^{2+}).

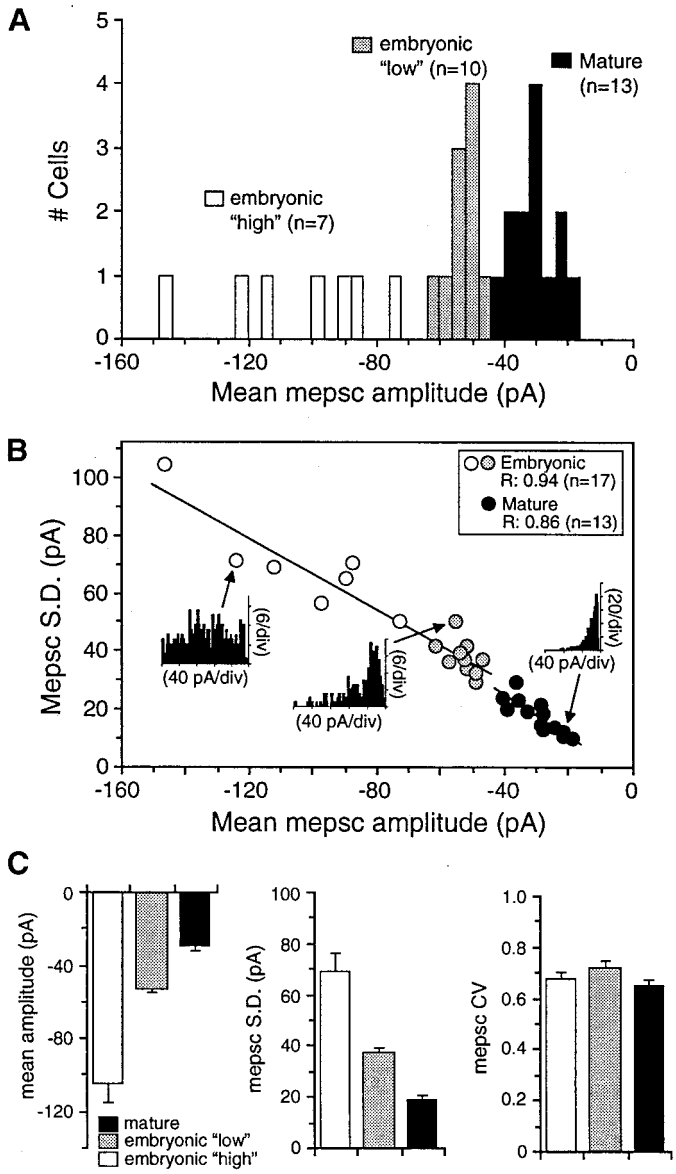

Figure 8. mEPSC amplitude and variability decrease with development. *A*, Histogram of mean mEPSC amplitudes recorded from embryonic and mature neurons (−70 mV; 1 mM Mg^{2+}). Mean mEPSC amplitudes at 13 mature synapses are tightly grouped (*filled bars*), with an average value of −30 ± 2 pA (n = 13). Embryonic mean mEPSC amplitudes appear to fall into two populations: a "low" group (n = 10; *shaded bars*) and a "high" group (n = 7; *open bars*), with an overall average amplitude of −74 ± 7 pA. *B*, Variability (SD) in mEPSC amplitude is plotted against the mean amplitude for 17 embryonic and 13 mature neurons. mEPSC variability is correlated strongly and positively with mean mEPSC amplitude; regression values in the *panel inset* were determined from straight line fits to the data. A much wider range of mEPSC amplitudes and variability is observed in embryonic neurons, which are plotted in two groups, as in *A*. *Inset* histograms show representative mEPSC amplitude distributions for a neuron from each group. *C*, Mean mEPSC amplitudes (*left panel*), variability in amplitude (SD, *middle panel*), and coefficients of variability ± SEM (CV; *right panel*) for the two embryonic groups and mature neurons shown in *A* and *B*. Mean mEPSC amplitude and variability are significantly larger in both embryonic groups than in mature mEPSCs, but there is no significant difference in CV during development.

Properties of embryonic AMPA-R synapses: larger mEPSC amplitude and variability and asynchronous multiquantal release

AMPA-R-mediated mEPSCs at embryonic spinal synapses have unusually large amplitudes and variability in TTX and frequently occur in unsynchronized bursts. mEPSC variability decreases with age, as observed at developing cerebellar (Wall and Usowicz, 1998) and hippocampal synapses (Hsia et al., 1998). However, our finding that mEPSC amplitude decreases by ~60% contrasts strikingly with studies at other developing central synapses (Wu et al., 1996; Gao et al., 1998; Hsia et al., 1998; Wall and Usowicz, 1998). Most embryonic mEPSCs are probably monoquantal, because their amplitude and variability are unchanged after reducing the probability of synchronous multiquantal fusion with 0-Ca^{2+} saline. By contrast, the dependence of bursts on external Ca^{2+} suggests that they are triggered by spontaneous presynaptic Ca^{2+} influx, resulting in episodes of unsynchronized multiquantal release. mEPSCs have similar amplitude and variability whether they occur in bursts or in isolation, indicating that they occur at the same population of synapses. This form of multiquantal release, which has not been described previously at a developing central synapse, may serve to increase the frequency of immature spontaneous synaptic currents to a functionally significant level.

Variability in miniature synaptic currents observed at many central synapses may derive from several factors, including intrinsic variability at individual synapses, synaptic heterogeneity such as different postsynaptic receptor densities, and multiquantal release (Bekkers et al., 1990; Borst et al., 1994; Bekkers and Stevens, 1995; Frerking et al., 1995, 1997; Liu and Tsien, 1995; Walmsley, 1995; Isaacson and Walmsley, 1996; Auger et al., 1998; Wall and Usowicz, 1998). The simplest explanation for our results is that embryonic DLi synapses have both greater variability and number of postsynaptic AMPA-R (Liu and Tsien, 1995; Wall and Usowicz, 1998) than at mature larval synapses. Postsynaptic AMPA-R and $GABA_A$ receptor number, respectively, underlie activity-modulated changes in mEPSC amplitude in cultured rat spinal neurons (O'Brien et al., 1998) and large variation in mIPSC amplitude in mouse cerebellar stellate cells (Nusser et al., 1997). However, embryonic AMPA-R that have greater conductance or are differently modulated (Benke et al., 1998) or differences in synaptic transmitter concentrations (Frerking et al., 1995; Kullmann and Asztely, 1998) also could contribute to mEPSC amplitude and variability. The large CV throughout development suggests that some combination of these factors maintains a large relative variability in quantal amplitude. Larval DLi receive excitatory input from up to three to four Rohon–Beard neurons, probably via *en passant* synaptic contacts, and have compact dendritic arbors (Soffe et al., 1984; Roberts et al., 1988; Sillar and Roberts, 1988). However, detailed synaptic structural features including synapse size, number, and distribution, which could correlate to functional developmental changes (Bennett et al., 1995; Walmsley et al., 1998), have not been examined. Determining whether mIPSCs undergo similar changes will determine whether similar mechanisms exist at embryonic inhibitory spinal synapses.

Ca^{2+} permeability of AMPA-R

Transmission mediated by Ca^{2+}-permeable AMPA-R has been reported at several mature synapses (Otis et al., 1995; Mahanty and Sah, 1998), but it is unclear how the expression of these receptors is regulated developmentally or whether they have a

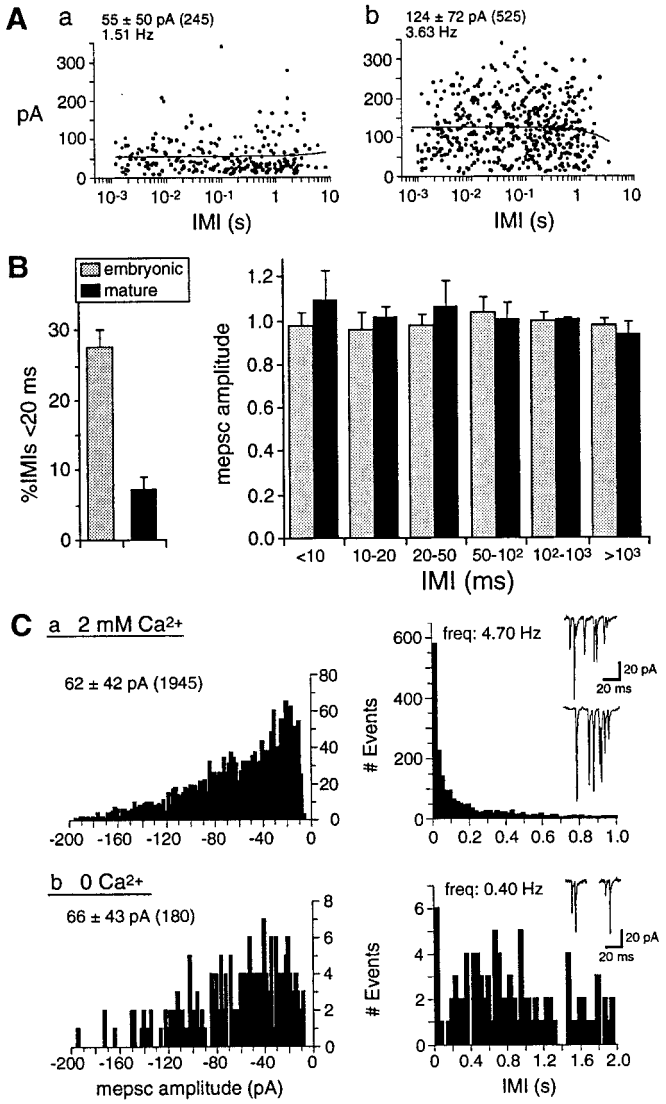

Figure 9. Ca^{2+}-dependent unsynchronized multiquantal release underlies mEPSC bursts at embryonic synapses. *A, B*, mEPSC amplitude at embryonic and mature synapses is independent of spontaneous frequency. *A*, Scatter plot of mEPSC amplitudes versus mEPSC intervals (IMI, in log scale) preceding each event for two embryonic neurons from the "low" (*a*) and "high" amplitude groups (*b*) shown in Figure 8. Mean mEPSC amplitudes ± SD, number of events, and frequency in each neuron are shown *above* the plots. mEPSCs occurring during bursts are those preceded by brief duration IMIs (<20 msec). There is no correlation between mEPSC amplitude and IMI, demonstrating that mEPSCs within and outside of bursts have similar amplitudes; lines were fit to the data by linear regression ($r = 0.008$, *a*; $r = -0.053$, *b*). *B, Left*, The proportion of brief duration IMIs (<20 msec) is significantly larger for embryonic (28 ± 3%) than for mature (7 ± 2%) synapses. Mean mEPSC frequencies ± SEM for the data shown are 3.3 ± 1.1 Hz for embryonic neurons (range, 0.7–9.9 Hz; $n = 8$) and 3.3 ± 1.3 Hz for mature neurons (range, 0.7–13.4 Hz; $n = 9$). *B, Right*, mEPSC amplitudes (normalized to the mean value in each recording ± SEM) are plotted against IMI bins of increasing duration for embryonic ($n = 8$) and mature neurons ($n = 9$). There is no significant difference in mEPSC amplitudes over a 1000-fold range of IMI duration, indicating that amplitude is not affected by intrinsic release frequency. *C*, Reducing the probability of spontaneous release eliminates most spontaneous bursts but does not alter mEPSC amplitude and variability. mEPSC amplitude (*left plots*) and IMI distributions (*right plots*) are shown for an embryonic neuron (40 hr) in normal 2 mM Ca^{2+} (*a*) and 0-Ca^{2+} saline (*b*). Mean amplitudes ± SD, number of events, and frequency for both conditions are shown *above* the plots. mEPSC amplitude and variability are not significantly different in 0-Ca^{2+} saline, but mEPSC frequency is reduced to <10% of control, and bursts of >2 mEPSCs are eliminated. Examples of normal mEPSC bursts and rare doublets in 0-Ca^{2+} are *inset above* the IMI histograms.

role at developing excitatory synapses *in vivo*. AMPA-R Ca^{2+} permeability in mammalian subunit coexpression studies is conferred by the lack of the edited GluR2 subunit isoform (for review, see Jonas and Burnashev, 1995). Relative Ca^{2+} permeabilities ($P_{Ca}/P_{monocation}$) from ~0.2 to ~2 reported for native Ca^{2+}-permeable AMPA-R, compared with values of 5–10 for NMDA-R (Mayer and Westbrook, 1987; Jahr and Stevens, 1993), presumably reflect different levels of GluR2-containing receptors (Jonas and Burnashev, 1995). AMPA-R in cultured embryonic *Xenopus* spinal neurons directly mediate Ca^{2+} influx (relative P_{Ca} ~1.9) as well as Ca^{2+} release from internal stores (Gleason and Spitzer, 1998). We show that Ca^{2+}-permeable AMPA-R (relative P_{Ca} ~1.7) are present at embryonic excitatory spinal synapses, as well as extrasynaptically. Mature DLi also express Ca^{2+}-permeable AMPA-R, although relative P_{Ca} (~1.0) is decreased as compared with embryonic DLi, potentially reflecting a change in AMPA-R subtype expression as synapses mature.

Development of glutamatergic signaling at *Xenopus* excitatory spinal synapses contrasts with other developing central synapses

Many immature excitatory synapses in mammalian hippocampus (Durand et al., 1996; Liao and Malinow, 1996; Liao et al., 1998; Petralia et al., 1998), sensory cortex (Crair and Malenka, 1995; Isaac et al., 1997; Golshani et al., 1998), and spinal motoneurons (Ziskind-Conhaim, 1990), as well as in *Xenopus* optic tectum (Wu et al., 1996), appear to lack functional AMPA-R. Initial transmission at these synapses is thus nearly or completely absent, except at strongly depolarized potentials or in Mg^{2+}-free saline that reveals NMDA-R currents or after LTP-inducing stimulation paradigms that "unsilence" synaptic AMPA-R (Liao et al., 1995; Durand et al., 1996; Wu et al., 1996; Isaac et al., 1997). A postnatal increase in AMPA-R synaptic currents (Crair and Malenka, 1995; Wu et al., 1996; Isaac et al., 1997) and a shortening of NMDA-R currents (Carmignoto and Vicini, 1992; Hestrin, 1992; Crair and Malenka, 1995) also occur at several mammalian central synapses. These studies support the view that NMDA-R activation is required for subsequent AMPA-R expression at most developing glutamatergic synapses (Constantine-Paton and Cline, 1998; Feldman and Knudsen, 1998), although they have not resolved how NMDA-R at immature silent synapses become sufficiently activated under physiological conditions to induce this expression.

In contrast, we find that AMPA-R-mediated mEPSCs predominate at immature *Xenopus* DLi glutamatergic spinal synapses and observe an opposite developmental transition in AMPA-R and NMDA-R currents. Why might these developing synapses depart from the above model? We propose that, at these and possibly other excitatory synapses, early expression of AMPA-R, particularly Ca^{2+}-permeable receptors, offers several advantages. Unlike sensory areas of the brain that undergo extensive synaptic integration and plasticity during a critical postnatal period, early spinal reflex and sensory-motor circuitry may be mainly "hard-wired," rendering initial NMDA-R activity less important than establishing functional motor output that enables early swimming and escape behaviors. AMPA-R mediate faster, larger-amplitude synaptic currents, ensuring early transmission. EPSPs in spinal

←

motoneurons and DLi in early *Xenopus* larvae have similarly prominent non-NMDA-R components (Clarke and Roberts, 1984; Dale and Roberts, 1985; Sillar and Roberts, 1988), indicating that AMPA-R are used preferentially at other embryonic excitatory synapses.

Our finding that embryonic mEPSCs have amplitudes ~2.5-fold larger than mature mEPSCs furthermore suggests that AMPA-R number is greater at immature synapses. AMPA-R density at cultured mammalian synapses has been shown to vary inversely with synapse number (Liu and Tsien, 1995) and to be downregulated by increased neuronal activity levels (Craig, 1998; O'Brien et al., 1998; Turrigiano et al., 1998). The developmental decrease in mEPSC amplitude therefore may coincide with increased neuronal activity and the number of synaptic inputs, and with a corresponding decrease in postsynaptic AMPA-R number.

Moreover, Ca^{2+}-permeable AMPA-R are likely to mediate postsynaptic Ca^{2+} signals at early stages when activity level and excitatory synapse number are probably low. Large mEPSCs occurring in spontaneous bursts provide a mechanism for amplifying and prolonging AMPA-R-mediated Ca^{2+} influx in the absence of action potentials. To our knowledge, functional Ca^{2+}-permeable AMPA-R have not been reported previously at immature glutamatergic synapses *in vivo*. However, Ca^{2+}-permeable AMPA-R support several forms of Ca^{2+}-dependent synaptic modulation independently of NMDA-R, including LTP (Gu et al., 1996; Jia et al., 1996; Mahanty and Sah; 1998). Therefore, it is plausible that developing synapses could use Ca^{2+}-permeable AMPA-R both for functional transmission and for Ca^{2+}-dependent modulatory processes usually dependent on NMDA-R.

These interpretations do not preclude a functional role for NMDA-R in the developing spinal cord. mEPSC distributions in Mg^{2+}-free saline indicate that NMDA-R are present at ~35 and ~80% of embryonic and mature larval synapses, respectively. NMDA-R-mediated EPSPs regulate interspike potential and the cycle period of postembryonic rhythmic swimming output (Dale, 1995), demonstrating that NMDA-R contribute to synaptic signaling under conditions that relieve voltage-dependent Mg^{2+} blockade. The postembryonic increase in the proportion of NMDA-R-expressing synapses parallels the period during which NMDA-R predominate at tectal synapses and may coincide with a later period of plasticity in the spinal cord, supporting experience-dependent modification of larval motor behavior. NMDA-R-mediated Ca^{2+} influx also may underlie chemotropic responses in developing *Xenopus* spinal neurons (Zheng et al., 1996). NMDA-R channel events often are recorded in embryonic as well as mature neurons even in the presence of Mg^{2+}, suggesting that NMDA-R activation by extrasynaptic glutamate diffusion (Kullmann and Asztely, 1998; Walmsley et al., 1998) may admit sufficient Ca^{2+} to serve such a role.

Our results suggest that different glutamatergic synapses meet developmental and functional requirements in different ways. Embryonic *Xenopus* excitatory spinal synapses are specialized to achieve functional transmission and generate postsynaptic Ca^{2+} signals via AMPA-R activation. Postsynaptically, embryonic AMPA-R are highly Ca^{2+}-permeable and mediate large-amplitude mEPSCs. Presynaptically, unsynchronized spontaneous multiquantal transmitter release prolongs receptor action. Large, fast synaptic currents ensure transmission and motor function beginning well before hatching, which may be important for the development of patterned swimming activity. AMPA-R-mediated Ca^{2+} signals are likely to have a role in synaptic differentiation, including the regulation of changes in postsynaptic receptor expression and function. Ca^{2+}-permeable AMPA-R thus may serve a primary role in transmission from early stages as well as regulatory roles analogous to those suggested for NMDA-R.

REFERENCES

Auger C, Kondo S, Marty A (1998) Multivesicular release at single functional sites in cerebellar stellate and basket cells. J Neurosci 18:4532–4547.

Bekkers JM, Stevens CF (1989) NMDA and non-NMDA receptors are colocalized at individual excitatory synapses in cultured rat hippocampus. Nature 341:230–233.

Bekkers JM, Stevens CF (1995) Quantal analysis of EPSCs recorded from small numbers of synapses in hippocampal cultures. J. Neurophysiol 73:1145–1156.

Bekkers JM, Richerson GB, Stevens CF (1990) Origin of variability in quantal size in cultured hippocampal neurons and hippocampal slices. Proc Natl Acad Sci USA 87:5359–5362.

Ben-Ari Y, Khazipov R, Leinekugel X, Caillard O, Gaiarsa JL (1997) $GABA_A$, NMDA, and AMPA receptors: a developmentally regulated "menage a trois." Trends Neurosci 20:523–529.

Benke TA, Luthi A, Isaac JT, Collingridge GL (1998) Modulation of AMPA receptor unitary conductance by synaptic activity. Nature 393:793–797.

Bennett MR, Gibson WG, Robinson J (1995) Probabilistic secretion of quanta: spontaneous release at active zones of varicosities, boutons, and endplates. Biophys J 69:42–56.

Borst JGG, Lodder JC, Kits KS (1994) Large amplitude variability of GABAergic IPSCs in melanotropes from *Xenopus laevis*: evidence that quantal size differs between synapses. J Neurophysiol 71:639–655.

Carmignoto G, Vicini S (1992) Activity-dependent decrease in NMDA receptor responses during development of the visual cortex. Science 258:1007–1011.

Clarke JDW, Roberts A (1984) Interneurones in the *Xenopus* embryo spinal cord: sensory excitation and activity during swimming. J Physiol (Lond) 354:345–362.

Constantine-Paton M, Cline HT (1998) LTP and activity-dependent synaptogenesis: the more alike they are, the more different they become. Curr Opin Neurobiol 8:139–148.

Craig AM (1998) Activity and synaptic receptor targeting: the long view. Neuron 21:459–462.

Crair MC, Malenka RC (1995) A critical period for long-term potentiation at thalamocortical synapses. Nature 375:325–328.

Dale N (1995) Experimentally derived model for the locomotor pattern generator in the *Xenopus* embryo. J Physiol (Lond) 489:489–510.

Dale N, Roberts A (1985) Dual-component amino-acid-mediated synaptic potentials: excitatory drive for swimming in *Xenopus* embryos. J Physiol (Lond) 363:35–59.

Donevan SD, Rogawski MA (1993) GYKI 53266, a 2,3-benzodiazepine, is a highly selective, noncompetitive antagonist of AMPA/kainate receptor responses. Neuron 10:51–59.

Durand GM, Kovalchuk Y, Konnerth A (1996) Long-term potentiation and functional synapse induction in developing hippocampus. Nature 381:71–75.

Feldman DE, Knudsen EI (1998) Experience-dependent plasticity and the maturation of glutamatergic synapses. Neuron 20:1067–1071.

Frerking M, Borges S, Wilson M (1995) Variation in GABA mini amplitude is the consequence of variation in transmitter concentration. Neuron 15:885–895.

Frerking M, Borges S, Wilson M (1997) Are some minis multiquantal? J Neurophysiol 78:1293–1304.

Gao BX, Cheng G, Ziskind-Conhaim L (1998) Development of spontaneous synaptic transmission in the rat spinal cord. J Neurophysiol 79:2277–2287.

Gilbertson TA, Scobey R, Wilson M (1991) Permeation of calcium ions through non-NMDA glutamate channels in retinal bipolar cells. Science 251:1613–1615.

Gleason EL, Spitzer NC (1998) AMPA and NMDA receptors expressed by differentiating *Xenopus* spinal neurons. J Neurophysiol 79:2986–2998.

Golshani P, Warren RA, Jones EG (1998) Progression of change in NMDA, non-NMDA, and metabotropic glutamate receptor function at the developing corticothalamic synapse. J Neurophysiol 80:143–154.

Gu JG, Albuquerque C, Lee CJ, MacDermott AB (1996) Synaptic strengthening through activation of Ca^{2+}-permeable AMPA receptors. Nature 381:793–796.

Hamill OP, Marty A, Neher E, Sigworth FJ (1981) Improved patch clamp techniques for high-resolution current recordings from cells and cell-free patches. Pflügers Arch 391:85–100.

Hestrin S (1992) Developmental regulation of NMDA-R-mediated synaptic currents at a central synapse. Nature 357:686–689.

Hori Y, Endo K (1994) Miniature postsynaptic currents recorded from identified rat spinal dorsal horn projection neurons in thin-slice preparations. Neurosci Lett 142:191–195.

Hsia AY, Malenka RC, Nicoll RA (1998) Development of excitatory circuitry in the hippocampus. J Neurophysiol 79:2013–2024.

Isaac JTR, Crair MC, Nicoll RA, Malenka RC (1997) Silent synapses during development of thalamocortical inputs. Neuron 18:269–280.

Isaacson JS, Walmsley B (1995) Receptors underlying excitatory synaptic transmission in slices of the rat anteroventral cochlear nucleus. J Neurophysiol 73:964–973.

Isaacson JS, Walmsley B (1996) Amplitude and time course of spontaneous and evoked excitatory postsynaptic currents in bushy cells of the anteroventral cochlear nucleus. J Neurophysiol 76:1566–1571.

Jahr CE, Stevens CF (1993) Calcium permeability of the *N*-methyl-D-aspartate receptor channel in hippocampal neurons in culture. Proc Natl Acad Sci USA 90:11573–11577.

Jia Z, Agopyan N, Miu P, Xiong Z, Henderson J, Gerlai R, Taverna FA, Velumian A, MacDonald J, Carlen P, Abramow-Newerly W, Roder J (1996) Enhanced LTP in mice deficient in the AMPA receptor GluR2. Neuron 17:945–956.

Johnson JW, Ascher P (1987) Glycine potentiates the NMDA response in cultured mouse brain neurons. Nature 325:529–531.

Jonas P, Burnashev N (1995) Molecular mechanisms controlling calcium entry through AMPA-type glutamate receptor channels. Neuron 15:987–990.

Kullmann DM, Asztely F (1998) Extrasynaptic glutamate spillover in the hippocampus: evidence and implications. Trends Neurosci 21:8–14.

Liao D, Malinow R (1996) Deficiency in induction but not expression of LTP in hippocampal slices from young rats. Learn Mem 3:138–149.

Liao D, Hessler NA, Malinow R (1995) Activation of postsynaptically silent synapses during pairing-induced LTP in CA1 region of hippocampal slices. Nature 375:400–404.

Liao D, Zhang X, O'Brien R, Ehlers MD, Huganir RL (1998) Regulation of morphological postsynaptic silent synapses in developing hippocampal neurons. Nat Neurosci 2:37–43.

Liu G, Tsien RW (1995) Properties of synaptic transmission at single hippocampal synaptic boutons. Nature 375:404–408.

Mahanty NK, Sah P (1998) Calcium-permeable AMPA receptors mediate long-term potentiation in interneurons in the amygdala. Nature 394:683–687.

Malenka RC, Nicoll RA (1997) Silent synapses speak up. Neuron 19:473–476.

Mayer ML, Westbrook GL (1987) Permeation and block of *N*-methyl-D-aspartic acid receptor channels by divalent cations in mouse cultured central neurones. J Physiol (Lond) 394:501–527.

Neher E (1992) Correction for liquid junction potentials in patch clamp experiments. Methods Enzymol 207:123–131.

Nicoll RA, Malenka RC, Kauer, JA (1990) Functional comparison of neurotransmitter receptor subtypes in mammalian central nervous system. Physiol Rev 70:513–565.

Nieuwkoop PD, Faber J (1967) Normal table of *Xenopus laevis* (Daudin): a systematical and chronological survey of the development from the fertilized egg till the end of metamorphosis, 2nd Ed. Amsterdam: North-Holland.

Nusser Z, Cull-Candy S, Farrant M (1997) Differences in synaptic $GABA_A$ receptor number underlie variation in GABA mini amplitude. Neuron 19:697–709.

O'Brien JA, Isaacson JS, Berger AJ (1997) NMDA and non-NMDA receptors are colocalized at excitatory synapses of rat hypoglossal motoneurons. Neurosci Lett 227:5–8.

O'Brien RJ, Kamboj S, Ehlers MD, Rosen KR, Fischbach GD, Huganir RL (1998) Activity-dependent modulation of synaptic AMPA receptor accumulation. Neuron 21:1067–1078.

Otis TS, Raman IM, Trussell LO (1995) AMPA receptors with high Ca^{2+} permeability mediate synaptic transmission in the avian auditory pathway. J Physiol (Lond) 482:309–315.

Paternain AV, Morales M, Lerma J (1995) Selective antagonism of AMPA receptors unmasks kainate receptor-mediated responses in hippocampal neurons. Neuron 14:185–189.

Petralia RS, Esteban JA, Wang Y-X, Partridge JG, Zhao H-M, Wenthold RJ, Malinow R (1998) Selective acquisition of AMPA receptors over postnatal development suggests a molecular basis for silent synapses. Nat Neurosci 2:31–36.

Roberts A, Clarke JDW (1982) The neuroanatomy of an amphibian embryo spinal cord. Philos Trans R Soc Lond [Biol] 296:195–212.

Roberts A, Dale N, Ottersen OP, Storm-Mathisen J (1988) Development and characterization of commissural interneurones in the spinal cord of *Xenopus laevis* embryos revealed by antibodies to glycine. Development 103:447–461.

Rohrbough J, Spitzer NC (1996) Regulation of $[Cl^-]_i$ by Na^+-dependent Cl^- cotransport distinguishes depolarizing from hyperpolarizing $GABA_A$ receptor-mediated responses in spinal neurons. J Neurosci 16:82–91.

Sheetz AJ, Constantine-Paton M (1994) Modulation of NMDA receptor function: implications for vertebrate neural development. FASEB J 8:745–752.

Sheetz AJ, Nairn AC, Constantine-Paton M (1997) *N*-methyl-D-aspartate receptor activation and visual activity induce elongation factor-2 phosphorylation in amphibian tecta: a role for *N*-methyl-D-aspartate receptors in controlling protein synthesis. Proc Natl Acad Sci USA 94:14770–14775.

Sillar KT, Roberts A (1988) Unmyelinated cutaneous afferent neurons activate two types of excitatory amino acid receptor in the spinal cord of *Xenopus laevis* embryos. J Neurosci 8:1350–1360.

Sillar KT, Roberts A (1991) Segregation of NMDA and non-NMDA receptors at separate synaptic contacts: evidence from spontaneous EPSPs in *Xenopus* embryo spinal neurones. Brain Res 545:24–32.

Sillar KT, Simmers J (1994) Presynaptic inhibition of primary afferent transmitter release by 5-hydroxytryptamine at a mechanosensory synapse in the vertebrate spinal cord. J Neurosci 14:2636–2647.

Soffe SR, Clarke JD, Roberts A (1984) Activity of commissural interneurons in spinal cord of *Xenopus* embryos. J Neurophysiol 151:1257–1267.

Turrigiano G, Leslie KR, Desai N, Rutherford LC, Nelson S (1998) Activity-dependent scaling of quantal amplitude in neocortical neurons. Nature 391:892–895.

van den Pol AN, Obrietan K, Cao V, Trombley PQ (1995) Embryonic hypothalamic expression of functional glutamate receptors. Neuroscience 67:419–439.

Vincent P, Marty A (1993) Neighboring cerebellar Purkinje cells communicate via retrograde inhibition of common presynaptic interneurons. Neuron 11:885–893.

Wall MJ, Usowicz MM (1998) Development of the quantal properties of evoked and spontaneous synaptic currents at a brain synapse. Nat Neurosci 1:675–682.

Walmsley B (1995) Interpretation of "quantal" peaks in distributions of evoked synaptic transmission at central synapses. Proc R Soc Lond [Biol] 261:245–250.

Walmsley B, Alvarez FJ, Fyffe REW (1998) Diversity of structure and function at mammalian central synapses. Trends Neurosci 21:81–88.

Wu G, Malinow R, Cline HT (1996) Maturation of a central glutamatergic synapse. Science 274:972–976.

Zhang Y, Auerbach A (1995) Kinetic properties of NMDA receptors in embryonic *Xenopus* spinal neurons. J Neurophysiol 74:153–161.

Zheng JQ, Wan JJ, Poo M-M (1996) Essential role of filopodia in chemotropic turning of nerve growth cone induced by a glutamate gradient. J Neurosci 16:1140–1149.

Ziskind-Conhaim L (1990) NMDA receptors mediate poly- and monosynaptic potentials in motoneurons of rat embryos. J Neurosci 10:125–135.

Zorumski CF, Yamada KA, Price MT, Olney JW (1993) A benzodiazepine recognition site associated with the non-NMDA glutamate receptor. Neuron 10:61–67.